Available online at www.sciencedirect.com
SCIENCE DIRECT
Journal of volcanology and geothermal research
ELSEVIER
Journal of Volcanology and Geothermal Research 154 (2006) 201–221
www.elsevier.com/locate/jvolgeores

Flowage differentiation in an andesitic dyke of the Motru Dyke Swarm (Southern Carpathians, Romania) inferred from AMS, CSD and geochemistry

Collin Nkono [a], Olivier Féménias [a,*], Hervé Diot [b], Tudor Berza [c], Daniel Demaiffe [a]

[a] *Laboratoire de Géochimie Isotopique et Géodynamique Chimique, DSTE, Université Libre de Bruxelles (CP 160/02) 50, av. Roosevelt 1050 Bruxelles, Belgium*
[b] *Université de La Rochelle, av. Crépeau, 17402 La Rochelle cedex 1, France. UMR CNRS 6112, UFR de Sciences et Techniques, BP 92208, 44322 Nantes Cedex 3 France*
[c] *Institutul Geologic al României, Bucureşti RO-12271, România*

Received 1 April 2005; received in revised form 23 December 2005; accepted 1 February 2006
Available online 20 March 2006

Abstract

Two dykes of different thickness (5.5 m for TJ31 and 23 m for TJ34) from the late Pan-African calc-alkaline Motru Dyke Swarm (S. Carpathians, Romania) have been studied by electron microprobe (mineral chemistry), crystal size distribution (CSD), anisotropy of magnetic susceptibility (AMS) and whole-rock geochemistry. All the physical and chemical variations observed across the dyke's width point to concordant results and show that the variations of both modal abundance and size of the amphibole and biotite microphenocrysts inside the dykes (deduced from the classical CSD measurements) are the result of a mechanical segregation of suspended crystals during magmatic transport. Despite a pene-contemporaneous regional tectonic, the flow-induced differentiation in the thicker dyke is characterized by the concentration of pre-existing Ti-rich pargasite-tschermakite, clinopyroxene and plagioclase crystals in the core of the dyke and of the extracted differentiated liquid near the walls. This mechanical differentiation induces a chemical differentiation with a basaltic andesite composition for the core of the dyke whereas the margins are andesitic. Thus the chilled margins appear as a slightly more evolved liquid with a Newtonian behaviour when compared to the average composition of the dyke. The localization of the liquid on both sides of the dyke has certainly facilitated the ascent of the central part of the dyke that behaved as a Binghamian mush.

Keywords: dyke; CSD; AMS; flowage differentiation; Romania

1. Introduction

Understanding of dyke emplacement mechanism is of major importance to study the feeder processes of volcanic eruptions and the magmatic evolution of lavas during their transport through the crust. Numerous observations have shown complex and various petrographic textures inside dykes (i.e. Winkler, 1949). Several mechanical and/or thermal processes have been proposed to explain the position and size variations of mineral phases across dykes. Both asymmetrical and symmetrical distribution fabrics have been observed and

* Corresponding author. Tel.: +32 2 650 22 54; fax: +32 2 650 22 26.
E-mail address: ofemenia@ulb.ac.be (O. Féménias).

0377-0273/$ - see front matter © 2006 Elsevier B.V. All rights reserved.
doi:10.1016/j.jvolgeores.2006.02.011

related to contemporaneous regional tectonic activity (Correa-Gomes et al., 2001; Féménias et al., 2004). In many cases, the crystal population is coarser grained in the core of the dyke than near its walls. Nevertheless, the interpretation of these fabrics remains based on two main approaches that are rarely discussed together:

(1) The modal and size mineral variations inside a dyke are the result of a mechanical segregation (Bagnold effect) during the magmatic transport. For a Newtonian mush, i.e. a magmatic medium containing from 8 to 30% of crystals (Bagnold, 1954; Bhattacharji and Smith, 1964; Bhattacharji, 1967; Bhattacharji and Hehru, 1972; Komar, 1972a,b, 1976; Barrière, 1976; Nicolas, 1992; Arbaret et al., 1996), the magmatic flow during dyke emplacement may indeed generate interaction among solid particles (the carried crystals) and between these particles and the wall.
(2) The modal and size mineral variations inside the dyke result from the timing of crystallization during the cooling of the magma, which is itself function of the thickness of the dyke. The thermal window favourable to the crystallization of a given phase stays open much longer in the core zone of a dyke than near the dyke's rims (i.e. Winkler, 1949; Cashman and Marsh, 1988; Marsh, 1988; Cashman, 1993; Marsh, 1998; Higgins, 2002; Zieg and Marsh, 2002). In the classical crystal size distribution (CSD) interpretations, it is generally implied that the magma does not contain any suspended crystals before cooling.

To illustrate this debate, this study has been focused on two dykes (TJ31 and TJ34) of the Romanian Motru Dyke Swarm (MDS). Each dyke has been the subject of mineralogical, petrological, chemical, as well as structural (by CSD and AMS, i.e. anisotropy of magnetic susceptibility) investigations. In view of our results, we propose to reconsider the geological interpretation of the CSD in a dynamic point of view by linking the mineral segregation induced by the flow to the chemical signature of the rocks that can significantly vary along the width of the dyke.

2. Geological setting

The two studied dykes belong to a large Late Pan-African calc-alkaline dyke swarm, the Motru Dyke

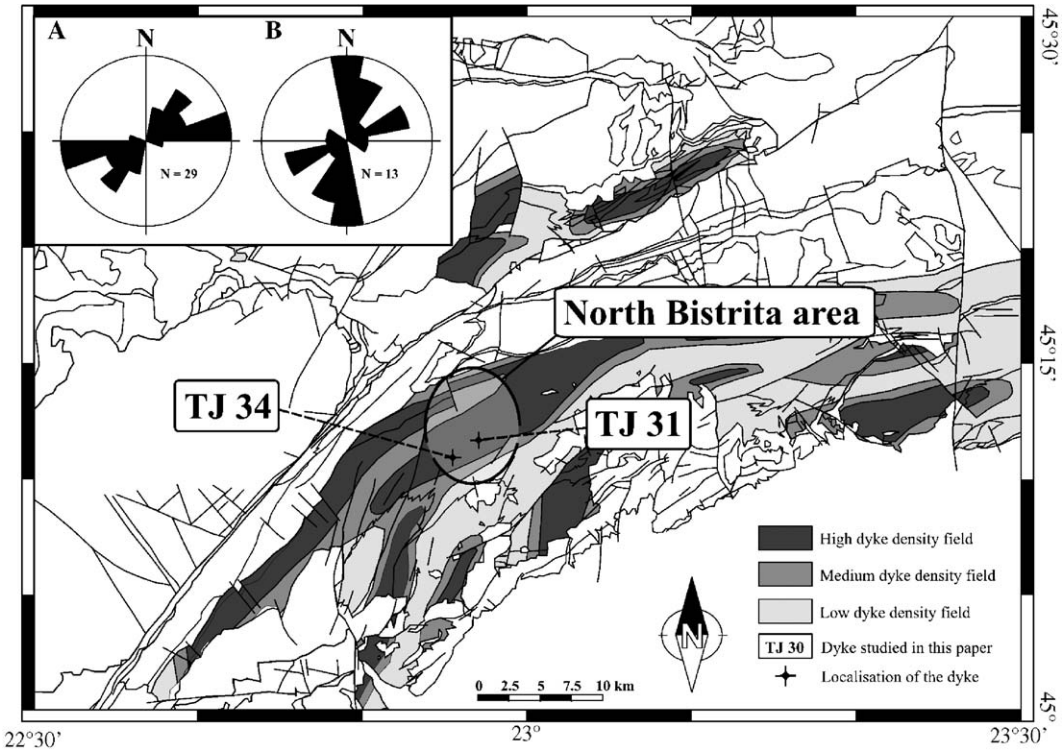

Fig. 1. Relative density distribution of the dykes of the Motru Dyke Swarm in the Lainici-Paius unit and location of the studied dykes (after Féménias et al., 2004). After 1/50,000 IGR map.

Swarm (MDS), which occurs in the Danubian window of the South Carpathian mountains in Romania. The MDS, first defined by Berza and Seghedi (1975), has recently been revisited (Féménias, 2003; Féménias et al., 2004). This dyke swarm is heterogeneously distributed in the field: some areas have a high density of dykes while others are almost free of dykes (Fig. 1). The high-density areas are regionally associated with a transcurrent regime during a late- to post-pan-African tectonic. Detailed field investigations have allowed to distinguish two populations of dykes which both crosscut the country rocks without chronological relations between them (no observation of continuity between them). The first population comprised thin dykes (< 1 m) with an N80° mean direction (Fig. 1A); the dykes of the second population are thicker (1 m up to several meters) with an N–S orientation (Fig. 1B). The two dykes studied in this paper (TJ31 and TJ34) came from the North Bistrița preserved area (Fig. 1). They belong to the second population. They have been chosen to illustrate the micro-porphyritic texture development common in the thick dykes.

3. Sampling and analytical procedures

For the two dykes, the contacts with the wall rocks are well exposed. Sampling intervals across dyke's width have been adapted according to their thickness. The 23 m thick TJ34 dyke has been sampled at 24 stations and the 5.5 m thick TJ31 dyke at 22 stations. Sampling has been performed with a portable drilling machine and, at each station, an oriented sample (25 mm diameter) has been cored.

The modal proportions (in vol.%) and crystal size distribution (CSD) of amphibole and biotite were determined on two-dimension polished thin sections (30 μm) cut into the drill core in a "normal orientation plane" (K_1–K_3) according to AMS results. These sections have already been correlated with the magmatic –Z directions of flow (Féménias et al., 2004). The numerical images (in polarised and polarised–analysed light) of the sample sections were acquired directly from the microscope by a digital camera. Because of the strong deuteritic and/or propylitic late emplacement alteration, the picturing of each mineral was done manually (Fig. 2) the crystals being identified using their crystallographic properties (natural colour, birefringence, twinning, cleavage, etc.). Crystal length and width were determined using a ruler on the micro-photographs. The measured area corresponds to a homogeneous zone of 280 mm^2. The size populations of the long axes of amphibole (TJ34 and TJ31), and biotite (TJ34) phenocrysts (Table 1) were corrected for two-dimensional–three-dimensional (2D–3D) effects

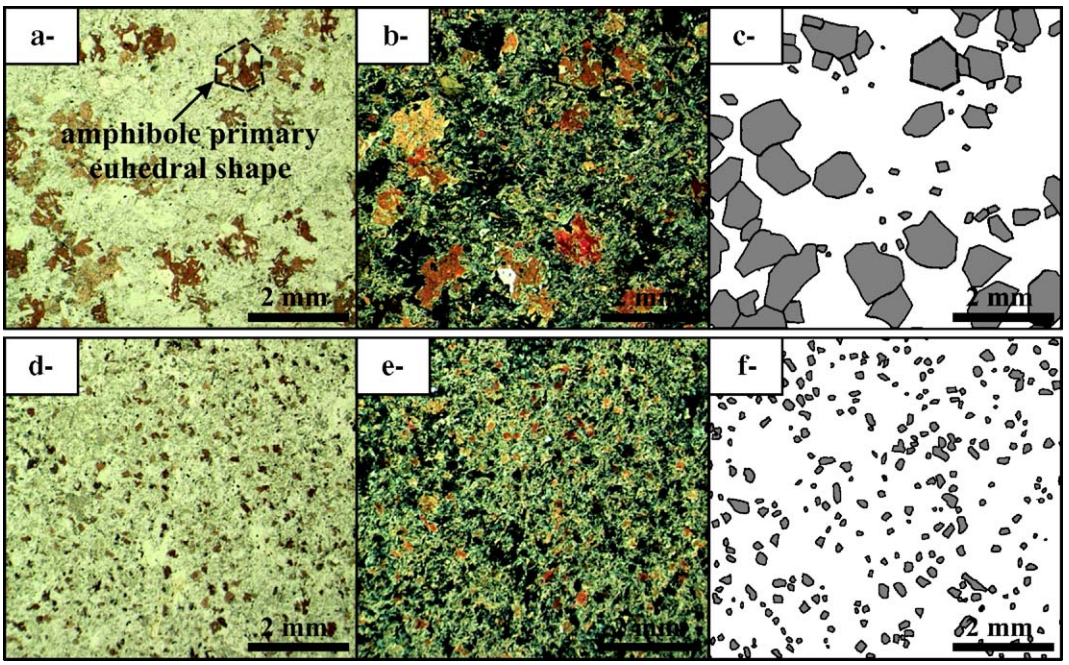

Fig. 2. The crystal sizes were manually counted on redrawn thin sections to take into account the original crystal size before deuteritisation. Close-up views of thin sections (plane-polarised light (a, d), cross-polarised light (b, e) and digitalized images (c, f) used for the CSD measurements) of two contrasted textures from the TJ31 dyke. Panels a, b and c come from TJ31k (x=325 cm). Panels d, e and f come from TJ31c (x=45 cm).

Table 1
Measured distribution of crystal size for amphibole (am) and biotite (bt) in each sample of the TJ31 and TJ34 dykes

Size (mm)		0.1	0.2	0.3	0.4	0.5	0.6	0.7	0.8	0.9	1	1.1	1.2	1.3	1.4	1.5	1.6	1.7	1.8	1.9	2	2.1	2.2	2.3	Nb
TJ31																									
b	Am	111	118	60	8	2	1	1																	301
c	Am	37	101	80	14	9	2	3	3																249
d	Am	25	58	61	44	16	5	3	2																214
e	Am	13	28	27	35	20	10	7	3																143
f	Am	10	20	19	33	22	11	7	4	2	3	2	1												134
g	Am	11	20	23	35	25	11	8	4	3	2	2	1												145
h	Am	10	14	14	14	25	11	9	4	3	3	3	2	1	1	1									115
i	Am	10	15	18	25	25	14	10	6	6	4	3	3	1											140
j	Am	10	15	12	15	21	16	11	7	6	4	3	2	2	1	1	1	1							128
k	Am	7	9	7	5	14	18	8	7	5	5	4	1	1	1	2	1	6	1	1	1				104
l	Am	3	3	8	11	21	20	18	11	7	4	4	3	2	1										116
m	Am	3	5	7	10	9	8	4	7	5	6	5	3	2	3	3	3	2	2	2	2	2	1	1	95
n	Am	0	0	3	5	6	7	7	8	10	9	5	5	4	4	5	3	1	1	1	1	1	1		87
o	Am	0	2	5	6	6	5	5	5	8	5	5	5	4	3	2	2	2	2	2	1	1	1		77
p	Am	1	2	14	7	16	11	6	10	5	8	4	2	2	1	1									90
q	Am	2	3	4	6	6	7	5	5	4	4	5	4	4	5	4	4	2	2	2	2	1			81
r	Am	5	16	19	19	19	21	19	13	11	9	6	5	3	3										168
s	Am	4	7	11	13	12	10	5	4	5	4	4	2	2	3	4	4	2	2	2	2	1			103
t	Am	0	15	32	28	40	29	13	7	6	6	6	6	3	2	2	2	1							198
u	Am	7	12	15	13	11	10	9	9	8	7	6	5	5	5	4	2	1							129
v	Am	26	43	55	49	38	29	21	15	5	3	3	2	1											290
TJ34																									
d	Bt	55	61	63	37	13	7																		236
e	Bt	32	47	40	20	8	7	3																	157
f	Bt	24	28	30	28	11	4																		125
g	Bt	18	23	28	25	15	7																		116
h	Bt	16	22	28	23	10	1																		100
i	Am	0	10	13	25	27	15	8	7	6	6	6	5	1	1	1									131
k	Am	0	0	14	28	29	15	8	6	5	4	2	2	1	1										115
l	Am	0	0	15	28	25	12	10	8	7	3	3													111
m	Am	0	0	21	29	20	11	8	6	6	5	4													110
n	Am	0	14	21	21	18	18	13	4	4	2	2													117
o	Am	0	19	21	23	21	13	9	5	4	2	2													119
p	Am	0	17	22	23	19	15	10	6	4	3	2													121
q	Am	0	18	21	27	21	15	4	3	1															110
r	Am	7	11	13	14	11	7	3																	66
s	Bt	12	17	19	11	7	4	3	1																74
t	Bt	37	51	47	20	7	1																		163
v	Bt	30	45	36	20	5																			136
w	Bt	45	55	30	13																				143

Nb: Total number of crystals measured on a surface of 280 mm^2.

using the method and software CSDCorrection v. 1.36 of Higgins (2000, 2002). This stereographic correction concerns both the intersection probability (section is more likely to intersect larger grains or crystals than smaller ones), and the cut section effect (one grain or crystal can produce different-sized sections in differently oriented cuts through a sample). Higgins (2000) developed this method of 2D–3D correction following the works of Saltikov (1967) and Sahagian and Proussevitch (1998) on stereological conversion of particle size distributions from 2D sections to actual 3D distributions. This method uses a quantification of the abovementioned 2D–3D effects to calculate a 3D size distribution. For the two mineral (amphibole and biotite) datasets (Table 1), the CSD parameters are given after correction (Table 2) using as shape parameters, the values 0.8–0.9–1.0 for the amphibole and 0.3–0.5–1.0 for the biotite, for a mean roundness of 0.8. The flow-related texture is clearly oriented and significant but as observed in several lavas studied by AMS it is not strong

Table 2
Measured crystal size distribution (CSD) and some parameters of the anisotropy of magnetic susceptibility (AMS) for the two dykes TJ31 and TJ34

	X (cm)		S (mm^{-1})	1σ	$n°$ (mm^{-4})	1σ	N_T	V (%)	1σ	K_m (μSI)	P'	T	K_1 az	K_1 inc	K_3 az	K_3 inc
TJ34																
a	20	Bt	–	–	–	–	–	–	–	317	1.03	0.55	261	56	119	28
b	45	Bt	–	–	–	–	–	–	–	380	1.06	0.29	262	64	101	24
c	80	Bt	–	–	–	–	–	–	–	335	1.03	0.37	236	60	115	17
d	150	Bt	− 5.3	0.4	3.8	0.2	3.6	3.8	0.8	392	1.04	0.11	260	67	119	18
e	180	Bt	− 5.5	0.5	3.4	0.3	2.2	2.9	0.9	421	1.04	0.32	259	74	108	14
f	270	Bt	− 4.5	0.6	2.7	0.3	1.7	2.3	0.6	365	1.05	0.39	224	64	118	7
g	375	Bt	− 3.4	0.6	2.1	0.4	1.4	2.6	0.6	440	1.04	0.42	268	67	124	19
h	520	Bt	− 4.6	0.7	2.6	0.4	1.3	1.8	0.5	398	1.06	0.38	250	56	119	24
i	640	Am	− 2.8	0.3	1.9	0.3	1.0	16.7	5.8	429	1.11	− 0.01	247	48	96	38
j	770	Am	–	–	–	–	–	–	–	604	1.09	− 0.13	273	59	109	30
k	900	Am	− 3.4	0.5	2.2	0.4	0.8	13.1	5.1	1058	1.21	− 0.11	285	63	103	27
l	1070	Am	− 3.6	0.5	2.2	0.4	0.7	10.6	3.6	446	1.16	0.08	253	59	109	26
m	1190	Am	− 3.2	0.4	1.8	0.4	0.8	11.5	3.4	1192	1.27	− 0.22	295	56	94	32
n	1370	Am	− 3.4	0.5	2.0	0.4	0.9	9.9	3.0	1058	1.36	− 0.21	279	47	118	41
o	1480	Am	− 3.9	0.5	2.3	0.4	1.1	8.8	3.3	546	1.03	0.27	235	60	122	13
p	1645	Am	− 3.7	0.5	2.2	0.4	1.1	9.6	3.5	392	1.02	0.18	247	54	117	25
q	1810	Am	− 4.3	0.7	2.5	0.4	1.1	6.3	2.1	360	1.02	0.63	273	66	118	22
r	1930	Am	− 3.8	0.9	1.7	0.5	0.7	3.1	1.1	376	1.04	0.32	268	50	126	34
s	2100	Bt	− 4.2	0.6	2.0	0.4	0.9	1.9	0.8	315	1.04	0.56	235	37	126	24
t	2250	Bt	− 4.3	0.6	2.9	0.3	2.1	2.7	0.5	361	1.09	0.62	230	35	118	28
u	2270	Bt	–	–	–	–	–	–	–	390	1.05	0.38	246	58	117	22
v	2290	Bt	− 6.7	0.8	3.7	0.4	1.9	1.6	0.5	524	1.03	0.52	221	65	113	25
w	2330	Bt	− 6.7	0.7	3.7	0.3	2.1	1.7	0.4	1085	1.34	0.28	248	46	118	32
x	2360	Bt	–	–	–	–	–	–	–	330	1.03	0.56	227	33	131	9
TJ31																
a	5	Am								479.0	1.03	0.21	337	43	137	45
b	25	Am	− 12.8	0.6	6.5	0.2	8.6	5.0	0.9	579.7	1.05	0.22	314	68	154	21
c	45	Am	− 8.3	0.6	4.8	0.2	3.2	6.1	1.3	531.0	1.03	0.21	315	60	147	29
d	75	Am	− 6.8	0.6	4.0	0.2	2.8	6.1	1.5	534.7	1.04	0.15	322	58	146	32
e	100	Am	− 4.5	0.6	2.6	0.3	1.5	6.5	1.7	485.8	1.04	0.14	298	59	134	31
f	125	Am	− 4.0	0.4	2.3	0.3	1.2	9.4	2.9	497.8	1.03	0.28	290	61	142	25
g	150	Am	− 3.9	0.4	2.3	0.3	1.4	9.8	3.0	542.0	1.03	0.00	300	69	141	20
h	185	Am	− 3.5	0.4	2.1	0.3	1.0	11.8	4.3	542.8	1.02	0.28	273	44	142	34
i	225	Am	− 3.1	0.4	1.9	0.3	1.2	13.2	3.6	543.9	1.04	0.28	300	48	144	39
j	275	Am	− 3.4	0.3	2.1	0.3	1.0	15.8	5.4	550.4	1.05	0.36	285	57	162	19
k	325	Am	− 2.6	0.3	1.6	0.4	0.4	20.8	8.9	525.6	1.02	0.35	272	53	137	29
l	355	Am	− 3.1	0.5	2.2	0.5	0.5	16.6	3.8	538.7	1.02	0.57	278	46	144	34
m	405	Am	− 1.6	0.3	0.1	0.4	0.5	30.2	11.0	538.8	1.04	0.72	263	34	139	40
n	425	Am	− 1.7	0.4	0.5	0.6	0.3	29.2	9.7	504.1	1.02	0.58	276	43	147	35
o	475	Am	− 1.8	0.3	0.2	0.4	0.3	26.7	7.7	482.5	1.02	0.59	263	23	150	42
p	485	Am	− 2.7	0.4	1.4	0.4	0.5	14.6	4.7	468.6	1.02	0.40	266	26	158	34
q	475	Am	− 1.6	0.3	0.2	0.4	0.3	28.6	7.9	506.0	1.03	0.16	266	46	136	32
r	495	Am	− 2.3	0.3	1.6	0.3	1.1	23.0	4.9	537.2	1.02	0.04	271	46	134	35
s	490	Am	− 1.6	0.2	0.3	0.3	0.6	26.0	7.8	690.3	1.02	− 0.08	312	63	132	27
t	495	Am	− 2.9	0.3	2.3	0.3	1.3	24.3	7.3	502.3	1.01	− 0.13	268	39	133	41
u	490	Am	− 2.2	0.3	1.1	0.3	0.9	24.6	7.1	671.6	1.03	0.45	334	41	155	49
v	527	Am	− 3.7	0.3	2.9	0.2	2.9	20.4	4.3	480.0	1.01	0.31	296	44	150	42

X (in cm) represents the distance to the western wall of the dyke. Bt: biotite-bearing and Am: amphibole-bearing. S: slope; $n°$: intercept; N_T: total number of crystals. K_m: mean magnetic susceptibility; P': anisotropy of magnetic ellipse; T: the shape parameter; K_1 az: azimuth of the maximum susceptibility axis; K_1 inc: inclination of the maximum susceptibility axis; K_3 az: azimuth of the minimum susceptibility axis; K_3 inc: inclination of the minimum susceptibility axis.

(a few percent) in the Motru dyke: for such a low anisotropy, the CSD results are not affected.

The AMS measurements were performed on the upper part of each drill core, cut into two or three 22-mm-high cylinders, using a Kappabridge KLY-3S susceptometer working in a weak alternative field whose resolution is better than 10^{-8} SI. For each cylinder, the measurement provides the magnitudes of the three principal, mutually orthogonal, axes of the AMS ellipsoid ($K_1 \geq K_2 \geq K_3$), as well as their azimuth and inclination with respect to the specimen frame. For each AMS station, the calculated averages of the magnitudes and orientations of the principal axes in the geographical frame have been reported in Table 2 and discussed in Section 5.

Major element compositions of amphibole have been determined by electron microprobe (Cameca SX50) at the Centre d'Analyses par Microsonde en Sciences de la Terre (CAMST, University of Louvain-la-Neuve) using a combination of natural and synthetic mineral standards. The operating conditions involve an accelerating voltage of 15 kV, a beam current of 20 nA and a count time of 10 s for Fe, Mn, Ti and Cr, 16 s for Si, Al, K and Mg, 24 s for Na.

For the TJ34 dyke, samples selected ($n=12$) for whole-rock major and trace elements have been crushed and ground in a stainless steel mortar. Whole-rock X-ray fluorescence (XRF) spectrometric analyses of major elements were made on fused glass discs at Liège University (Collectif de Géochimie instrumentale). Samples were pre-ignited at 1000 °C during 3 h, so major elements are reported on a volatile-free basis and total iron is reported as Fe_2O_3 (tot). The XRF measurements were calibrated using 22 international standards, the typical precision and accuracy (illustrated by the Relative Standard Deviation, RSD) for the major elements XRF analyses range from 0.1 to 1%. Some trace elements (Rb, Sr, Zr, Y, Nb, Th, Pb, Cu, Ni, Co, Zn and Ga) were measured by X-ray fluorescence spectrometry on pressed powder pellets. Data are reported in Table 3.

4. Petrology of the dykes

4.1. Petrography and mineralogy of the dykes

The MDS is composed of metaluminous high-K calc-alkaline subvolcanic dykes (Fig. 3). Most have andesitic

Table 3
Bulk-rock analyses of representative samples from the TJ34 andesitic dyke (Bt: biotite-bearing; Am: amphibole-bearing)

TJ 34	a and b	d	f	h	j	m	n	o	q	t	v	x
	Bt	Bt	Bt	Bt	Am	Am	Am	Am	Am	Bt	Bt	Bt
Major element [wt.%]												
SiO_2	58.12	58.68	58.73	58.41	56.53	56.70	56.07	56.98	57.11	57.81	57.91	58.63
TiO_2	0.89	0.84	0.83	0.76	0.84	0.80	0.78	0.81	0.74	0.89	0.87	0.85
Al_2O_3	18.01	17.64	17.62	16.15	16.10	16.11	15.81	16.06	15.86	18.44	18.07	18.15
Fe_2O_3t	6.50	6.07	6.24	6.10	7.06	6.82	6.75	6.98	6.73	6.64	6.39	6.51
MnO	0.10	0.10	0.10	0.10	0.12	0.11	0.12	0.12	0.13	0.11	0.10	0.10
MgO	4.00	3.81	4.17	5.91	6.95	7.03	7.36	7.21	7.25	4.51	4.12	4.17
CaO	6.26	6.61	6.76	7.25	7.51	7.48	7.83	7.12	6.98	5.88	6.50	5.64
Na_2O	3.60	3.77	3.72	3.31	3.05	3.16	2.96	3.06	4.23	3.56	3.57	3.72
K_2O	1.89	1.65	1.38	1.38	1.21	1.22	1.30	1.26	0.99	1.68	1.85	1.63
P_2O_5	0.15	0.15	0.15	0.13	0.14	0.14	0.13	0.14	0.12	0.15	0.15	0.15
Sum	99.5	99.3	99.7	99.5	99.5	99.6	99.1	99.7	100.1	99.7	99.5	99.6
Trace element [ppm]												
Co	25	22	22	29	32	33	34	35	31	26	24	24
Ni	4	5	6	12	13	15	16	19	18	5	3	4
Cu	9	7	6	5	9	14	10	16	6	6	10	11
Zn	67	68	72	65	69	65	67	69	68	71	67	65
Ga	20	19	19	17	17	17	17	18	17	20	19	20
Rb	65	56	46	43	39	38	41	41	36	63	64	64
Sr	346	357	365	328	314	319	326	303	230	317	341	300
Y	22	22	21	20	19	20	20	20	19	22	22	23
Zr	150	161	154	138	138	135	132	138	126	146	150	156
Nb	7.6	8.1	7.8	6.5	8.0	7.2	7.0	6.8	6.6	7.4	6.6	7.5
Pb	9.0	7.4	7.9	6.1	7.8	7.9	6.7	7.6	8.3	7.8	10.9	9.6
Th	4.7	5.5	5.4	4.3	4.6	2.5	1.9	3.5	3.4	5.8	4.6	5.1

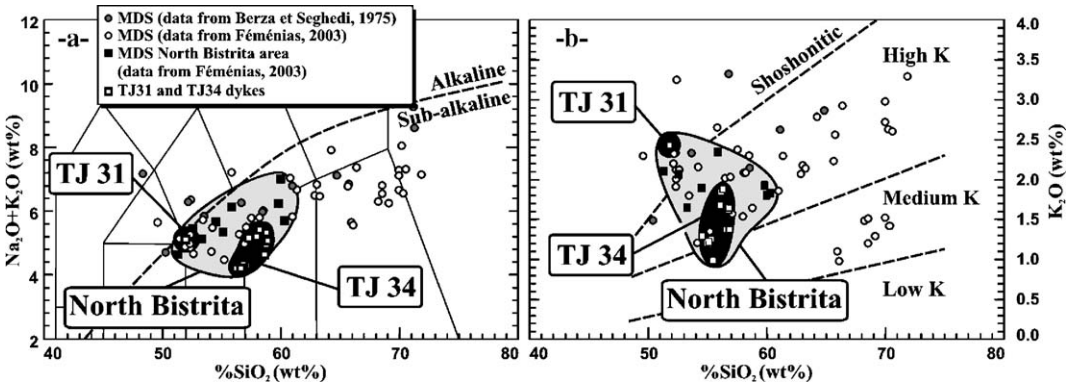

Fig. 3. Whole-rock chemical compositions of the Motru Dyke Swarm. a) Na_2O+K_2O (wt.%) vs. SiO_2. Nomenclature domains are from Le Bas et al. (1986) and Le Maitre (2002); the subalkaline–alkaline boundary is from Irvine and Baragar (1971). b) K_2O (wt.%) vs. SiO_2. Domain boundaries are from Rickwood (1989). The black area represents the two studied dykes; the grey area represents the composition field of the dykes from the North Bistrița area.

to dacitic composition; basaltic andesite and rhyolite are less common. The two studied dykes (TJ31 and TJ34) belong to the North Bistrița area that is essentially composed of basaltic andesite to andesite (Fig. 3). The observed textures are aphyric to micro-porphyritic. Porphyritic andesites contain euhedral brown amphibole and/or plagioclase microphenocrysts, while porphyritic dacites display euhedral plagioclase, magnesiohornblende and/or partly resorbed quartz. Plagioclase is often deeply retrogressed to epidote± calcite±white mica, it commonly appears as ghost phase. The groundmass consists of tiny quartz, plagioclase, ferromagnesian phases (amphibole and rarely clinopyroxene), oxides and devitrified glass (fine-grained deuteritic paragenesis). Mn-rich ilmenite is the main oxide; it occurs either as euhedral to subhedral crystals in glomeromorphic assemblages (mean grain size: 100–400 μm) or as single tiny (a few tens to hundred μm) anhedral to skeletal grains. Deuteritisation and propylitisation occur during and/or just after dyke emplacement and induce a low temperature/low pressure secondary paragenesis. Locally, Ti-bearing silicate phases have been pseudomorphosed to leucoxene; chlorite, calcite, talc, epidote and pyrrhotite-pyrite (altered to goethite and hematite) developed locally as millimeter-size euhedral grains.

TJ31 is micro-porphyritic basaltic andesite with brown amphibole and scarce pyroxene microphenocrysts. Clinopyroxene is either fresh or replaced by chlorite pseudomorphs. Plagioclase (< 2 mm) and clinopyroxenes are always deeply retrogressed; they have not been counted for CSD. TJ34 is fine-grained, biotite- and amphibole-bearing basaltic andesite to andesite with scarce sulphides and oxides in the core of the body. TJ31 is mineralogically homogeneous. On the other hand, TJ34 shows a heterogeneous distribution of oxides and ferromagnesian phases: biotite is present in the marginal zone while the central porphyritic zone is biotite-free and composed of amphibole and strongly altered clinopyroxene and plagioclase in a fine-grained deuteritic groundmass. A

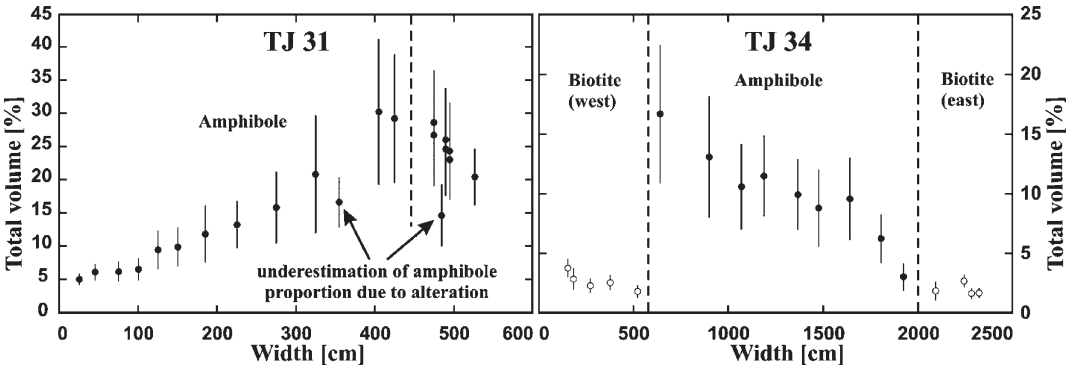

Fig. 4. Variation of the modal proportions (vol.%) of amphibole (black circle) and biotite (open circle) microphenocrysts across the two dykes (TJ31 and TJ34).

transitional zone with coexisting biotite and amphibole has been observed on each side of the amphibole-bearing central zone.

The two dykes have chilled margins implying a high level (subvolcanic) of emplacement. These margins contain of few microphenocrysts (amphibole and clinopyroxene in TJ31 plagioclase and biotite in TJ34) in a secondary (i.e. deuteritic) groundmass.

In the two dykes, the principal ferromagnesian phase is a euhedral brown amphibole, a Ti-rich pargasite-tschermakite (according to the IMA classification — Leake et al., 1997). The P–T conditions (0.6±0.1 GPa, 1000–900 °C for andesitic basalts to 700–600 °C for dacites) were those prevailing in a deep magma chamber, before the emplacement and cooling (Féménias et al., 2006) of the dyke in subvolcanic environment.

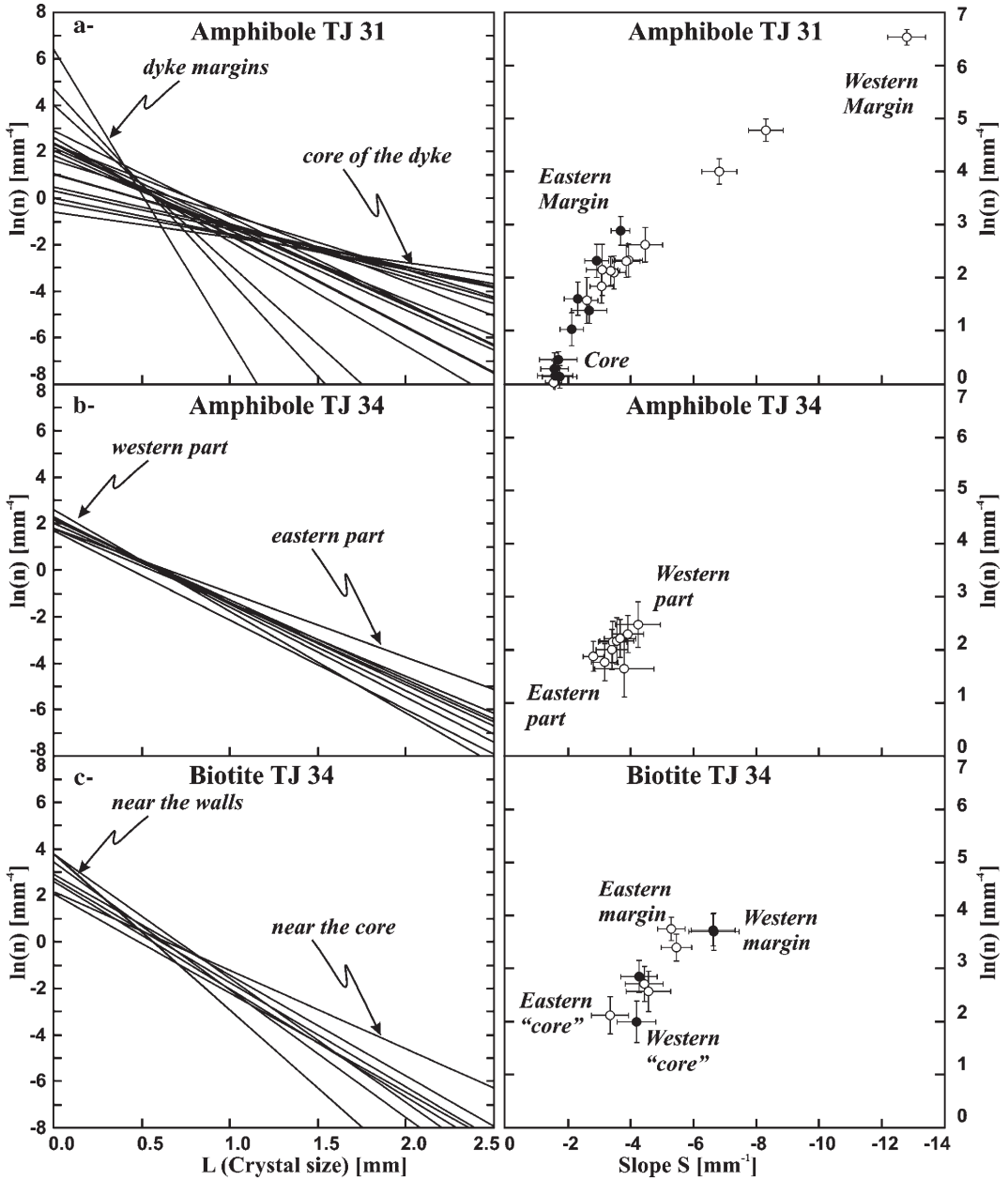

Fig. 5. The crystal size distribution of amphibole and biotite microphenocrysts in the TJ31 and TJ34 dykes shows typical fans and law distributions. a) CSD of amphibole in TJ31, b) CSD of amphibole in TJ34, c) CSD of biotite in TJ34. For a and c, the position of a line in the fan is strongly correlated with the position of the sample in the dyke.

According to the calibration of Wones and Eugster (1965), the biotites from TJ34 have crystallized at a relatively lower temperature (600 °C < T < 680 °C) that could be related to crystallization conditions inside the dyke during its cooling.

4.2. Modal abundances and crystal size distribution (CSD)

The modal abundances of amphibole and biotite have been estimated from the CSD data. In TJ31, the modal proportion of amphibole varies largely from ~5 vol.% near the western margin to a maximum of ~30 vol.% in the core, then abruptly decreases to ~20 vol.% (Table 2, Fig. 4). The petrographic core of the body, defined by the highest modal proportion of amphibole, is strongly shifted to the east. Samples l (355 cm) and p (485 cm) have significant lower amphibole content than their direct neighbours. This presumably reflects an underestimation of the amphibole abundance due to the stronger deuteritic alteration of the samples. TJ34 appears symmetrical but consists of two distinct zones. The external parts (~5 m on both margin) do not contain any amphibole phenocryst; biotite is the only ferromagnesian phase. Its low modal proportions (< 4 vol.%) do not show simple evolution versus distance from the wall (Table 2, Fig. 4). The central part of the dyke has only amphibole phenocrysts. The transition between these two mineralogical domains is quite sharp: there is a 10-cm-wide transitional zone with coexisting biotite and amphibole. The central biotite-free zone displays an asymmetrical distribution of amphibole grains, with modal proportion decreasing continuously from 16.7 to 3.1 vol.%.

The complete statistical results of the amphibole and biotite crystal populations from the two dykes are presented on Tables 1 and 2. Following the general convention, CSD data are plotted as linear crystal size (L [mm]) vs. logarithmic population density (ln(n) [mm^{-4}]; Marsh, 1998; Higgins, 2000); a log 10-decade scale with 5 to 8 intervals per decade has been used for the CSD 2D–3D correction. The CSD lines for the TJ34 biotites and the amphibole of the two dykes are mathematically usable: the "goodness of fit" values are all strictly lower than 1. These lines exhibit a log linear distribution over the whole range of grain sizes (Fig. 5). Each sample is thus characterized by a given line defined by the slope (S) and intercept ($n°$) parameters

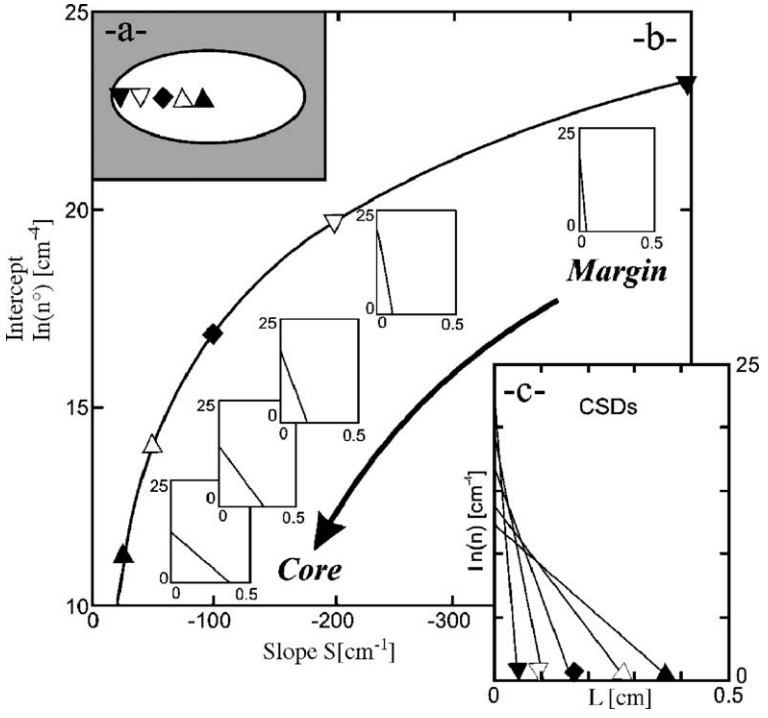

Fig. 6. Application of intercept slope equation and relation between CSD and the sample position within an intrusion (a-) after Zieg and Marsh (2002). Each point along the curve (b-) represents an idealized CSD. Moving along the curve corresponds to a change of the sample position within the intrusion (a-), or to a change of the cooling history of the magma. When a series of predicted CSDs is plotted together, they form a fan line distribution (c-).

(Fig. 5). The slope is proportional to the deviation of the population around the dominant crystal size, which is often described as a measure of growth rate and/or growth time. The intercept corresponds to the extrapolated number of grains of a population when the crystal size (L) tends towards zero; this is often considered as the nucleation density of the crystals. Taken altogether, the amphibole populations of TJ31 show a fanning distribution reflecting systematic variations between the core and the margins of the dyke. Such distributions are commonly described for igneous bodies such as laccoliths, lavas flows, sills and dykes (i.e. Cashman and Marsh, 1988; Mangan, 1990; Cashman, 1992; Mangan and Marsh, 1992; Resmini and Marsh, 1995; Higgins, 1996; Marsh, 1998; Marsh and Liu, 1999; Zieg and Marsh, 2002; Mock et al., 2003). The position of an individual CSD line within the fan is related to its stratigraphic position within the intrusion (Fig. 6, after Zieg and Marsh, 2002), and therefore, in numerous cases, to the cooling history of the sample. Fanning distributions are significantly less marked for the biotite and amphibole populations of the TJ34 dyke (Fig. 5).

These parameters are mathematically linked to the total number of crystals per volume unit (N_T). Across the dyke, the total volume (V) and the slope (S) of the TJ31 amphibole populations both increase (Table 2 and Fig. 7) with decreasing intercept ($n°$) and total number (N_T). The highest values of S correspond to the petrographic core deduced from the modal abundance of amphibole (see Fig. 4) and not to the geometric centre of the dyke at a width of ~275 cm (half thickness). The highest values of N_T and $n°$ characterize the two margins (respectively 8.6 and 6.5 on the western rim; 2.9 and 2.9 on the eastern rim); the lowest N_T value (0.3) is recorded in the "petrographic core" (sample TJ31 n). These parameters display a continuous evolution from one margin to the other, except for the two underestimated amphibole populations of samples TJ31 l (355 cm) and TJ31 p (485 cm) and for the western margin TJ31 b. All the CSD parameters show extreme values near the

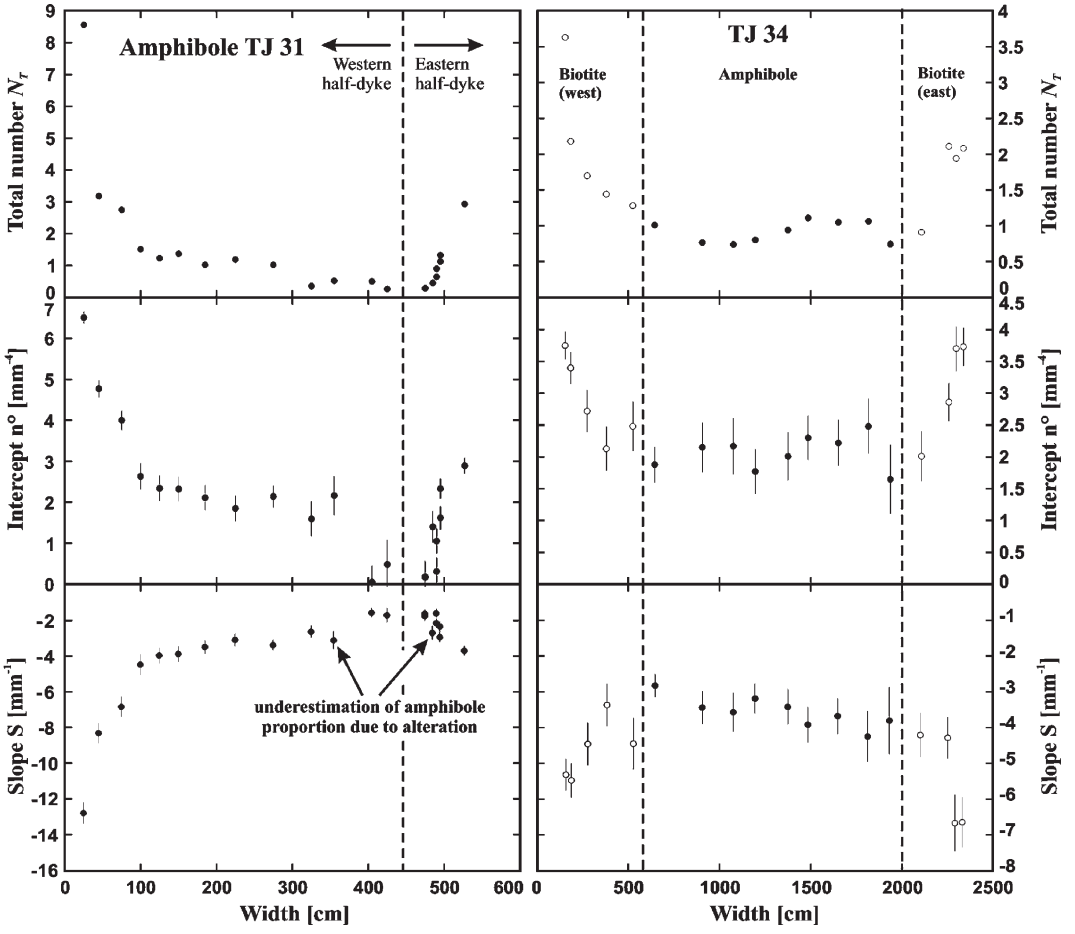

Fig. 7. Variation of some CSD parameters (N_T, $n°$ and S) within the two dyke bodies. Error bars represent 1σ deviation.

western margin of the dyke, they can probably be linked to a quenching effect near the wall. In that case, the very high values of N_T, $n°$ and the very low values of S (Table 2, Fig. 7) could be partially enhanced by the limitations of the measurement procedure for very small size (Table 1) and/or by the presence of quench crystals as suggested by Cashman and Marsh (1988). TJ31 is therefore characterized by an uncommon asymmetrical amphibole CSD fabric.

In the TJ34 dyke, at first sight, the amphibole population is roughly homogeneous: each CSD line (each sample) shows similar slope and intercept (Figs. 5 and 7). All the lines are roughly sub-parallel (Fig. 5), with $S \sim -3.5 \pm 0.5$ and $n° \sim 2.1 \pm 0.4$. On the contrary the biotite CSD shows a fan distribution and significant lateral variation of CSD values across the dyke. In details, the amphibole population only displays slight variation in the total number N_T (from 0.7 to 1.1) from the core zone to the transition zones with biotite (Table 2 and Fig. 7). These biotite populations are characterized by higher N_T and $n°$ and lower S values near the margins of the dyke (respectively 3.6 and 2.1; 3.8 and 3.7; − 5.3 and − 6.7) and lower N_T and $n°$ and higher S values near the central amphibole zone (respectively 1.3 and 0.9; 2.6 and 2.0; − 4.6 and − 4.2).

5. AMS investigation

5.1. Short presentation of the method

The kinematics of lava flow, recorded in the solidified rock as foliation and lineation, gives information on the late stage of fabric history (Fernandez and Laporte, 1991; Nicolas, 1992) and on flow direction in dykes (Archanjo et al., 2000; Féménias et al., 2004). Sheet-like bodies form when magma rises into an existing fracture, or creates a new crack by forcing its way through existing rock, and then solidify. Emplacement in a given tectonic setting records a local differential stress involving the combined effects of both external (faulting) and internal (magma pulse) stress fields (Correa-Gomes et al., 2001; Féménias et al., 2004). Deuteritic and/or propylitic fine-grained assemblages and micro-porphyritic subvolcanic textures of the

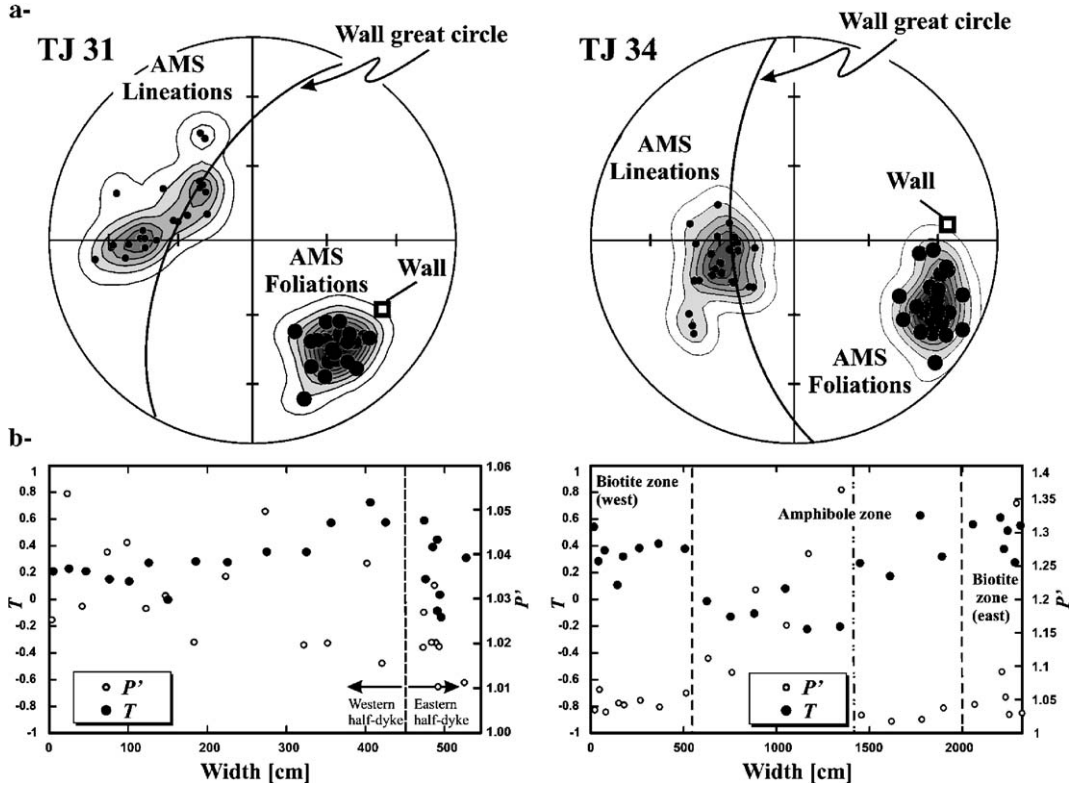

Fig. 8. Anisotropy of magnetic susceptibility (AMS) results. a) Stereographic representation (lower hemisphere) of the pole of the foliation (K_3) and lineation (K_1) in each dyke. Note -i) the obliquity between the wall direction and the magnetic foliation discussed in the text and in Féménias et al. (2004) and -ii) the position of the lineation around an average position down the dip of the foliation; b) Variations of the magnetic parameters T and P' versus position of the sample within the dyke.

MDS are not usable for a complete study of the fabric using image analysis method (i.e. shape-preferred orientation). Moreover, microscopic and macroscopic flow indicators are scarce (i.e. ordered orientation and/or gathering of crystals). Fortunately field and/or petrographic studies of shape-preferred orientations (SPO) of crystals can be completed by the fabric measurements of the magnetic mineralogy by the anisotropy of magnetic susceptibility (AMS) method. This method is indeed sensitive enough to determine the subtle fabrics in lava flows, which scarcely exceeds a few percent of anisotropy (Knight and Walker, 1988; Cañón-Tapia et al., 1996; Archanjo et al., 2000; Callot et al., 2001). Magnetic fabric has also been investigated in numerous cases and appears to be a good subfabric of the real magmatic fabric (bulk shape-preferred orientation of crystals in a magmatic medium).

5.2. AMS results

The magnetic fabric and the relations between the two populations of dykes have already been discussed in a previous AMS study (Féménias et al., 2004) in which the TJ34 dyke, one of the widest dykes of the N–S population, has been partially presented.

5.2.1. Magnetic susceptibility and anisotropy

The bulk magnetic susceptibility magnitude K_m, given by the arithmetic average of the K_1, K_2 and K_3 lengths of the AMS ellipsoid, ranges from 317 to 1192 μSI in TJ34 and from 465 to 690 μSI in TJ31 (Table 2): mean values are 465 and 533 μSI respectively. There is a bimodal frequency distribution of K_m values as already noted for the whole MDS (Féménias et al., 2004). This range 300–500 μSI (the most abundant) is representative of paramagnetic phases (amphibole and biotite) as the principal contributors to bulk susceptibility. Indeed in the two dykes, the K_m values are roughly correlated with the modal proportions of mafic phases and well correlated with the Fe_2O_3t content of the rocks (Table 3 for TJ34). The higher K_m values (> 500 μSI) of some samples could presumably be due to the contribution of secondary (propylitic) sulphide and associated hematite recognized in these samples. The pyrrhotite-pyrite development and its localization in the amphibole-bearing central zone of TJ34 are presumably related to the iron remobilisation during retrogression of the primary ferromagnesian silicate phases; this could have enhanced the primary magnetic signal originally due to the amphibole contribution. Extremely localized (only 6 stations) and without any influence on the orientation of the AMS ellipsoid axes, this secondary mineralogy mimics the first magnetic fabric acquired during the dyke emplacement. Thus, K_m variations from sample to sample and from rim to core in the two dykes could be attributed to two processes: (1) the variations of the modal proportions of amphibole and/or biotite microphenocrysts; and (2) the localization of a late-

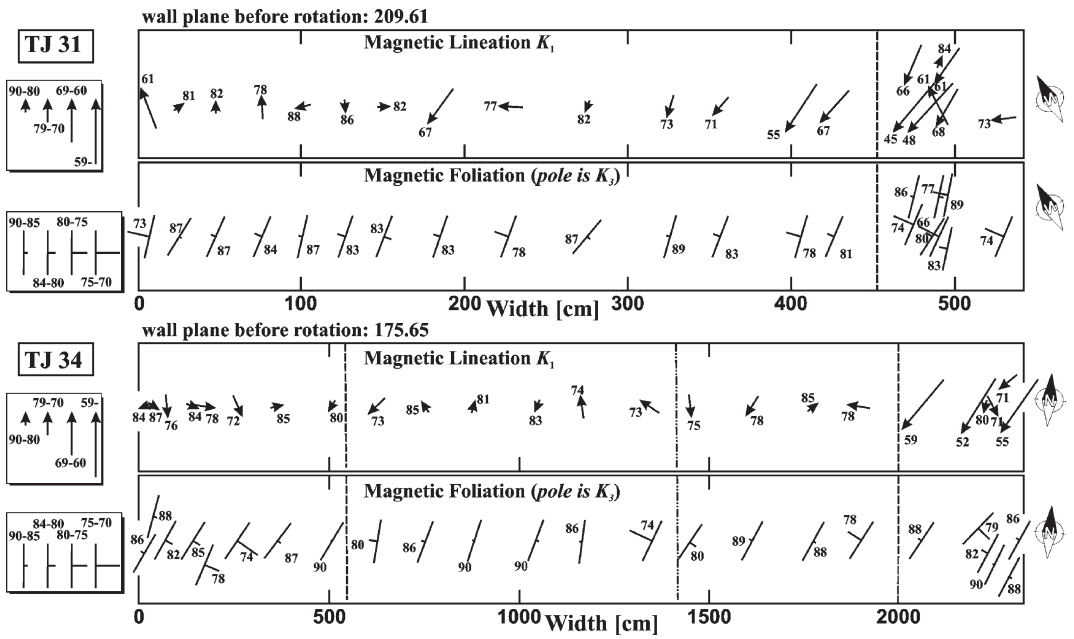

Fig. 9. Disposition of the magnetic lineation and foliation in the dykes TJ31 and TJ34 with an N–S vertical representation of the walls.

emplacement fluid percolation along channelled conduits that induced the crystallization of propylitic iron sulphide and associated hematite.

5.2.2. Intensity and shape of the magnetic fabric

The parameters P' and T ($P'=\exp[2((\ln K_1/K_m)^2+(\ln K_2/K_m)^2+(\ln K_3/K_m)^2)]^{1/2}$ and $T=(2(\ln K_2-\ln K_3)/(\ln K_1-\ln K_3))-1$), defined by Jelinek (1981), were calculated for the different AMS stations. P' describes the strength, or anisotropy degree, of the magnetic fabric and varies from $P'=1$ for an isotropic, spherical AMS ellipsoid to infinity. The shape parameter T varies from a prolate shape for $-1\le T<0$ (cigar-shaped for $T=-1$, i.e. $K_2=K_3$) to an oblate shape for $0<T\le 1$ (pancake-shaped for $T=1$, i.e. $K_1=K_2$) (Hrouda, 1982).

For our dykes, the range of P' values is quite large (1.01 to 1.36; Table 2 and Fig. 8), with an average of 1.1 for TJ34 and 1.04 for TJ31. Most P' values are in the narrow range 1.01 to 1.1, that is similar to the values reported for basaltic dykes (Raposo and D'Agrella-Filho, 2000). TJ34 displays the largest range of variations and there is a good correlation between the position of the samples in the dyke (i.e. the petrographic zoning) and the P' value (Fig. 8b) that regularly increases from the western rim to the core (from 1.03 to 1.36), then suddenly decreases to 1.03 and starts again to increase very slowly toward the eastern rim. In fact, there seems to be a sharp boundary, inside the central (amphibole-bearing) zone suggesting kinematics step between the eastern and western parts of the dyke. This structural (AMS) boundary ($x\approx 1400$ cm from the western boundary, between stations TJ34n and TJ34o) is clearly shifted compared to the mineralogical boundaries.

In TJ31, P' values are nearly constant and are not as high as in TJ34; they slightly decrease from the western margin ($P'\sim 1.04$) to the eastern one ($P'\sim 1.01$).

The T values range from -0.22 to 0.72 (Fig. 8 and Table 2) with an average of ~ 0.28 for the two dykes, indicating a planolinear to oblate AMS ellipsoid for the whole set of samples. P' and T parameters vary together through the dykes: for TJ31, the variation is only perceptible for the lowest P' values of the eastern boundary.

For TJ34 on the contrary, the values evolve from high T–low P' in the external domain to low T–high P' in the western amphibole zone. These contrasting domains are only apparent in the AMS parameters; they could be attributed to higher modal proportions of crystals. This structural central limit of the amphibole zone defined mainly by P' variations also corresponds clearly to a step regarding T values (Fig. 8b).

Paradoxically, these high P' and low T values of western part of the central amphibole zone of TJ34 (Fig. 8b) are found in a relatively undeformed core. We suggest that the fabric of the core zone has already acquired and frozen during the early evolution of the

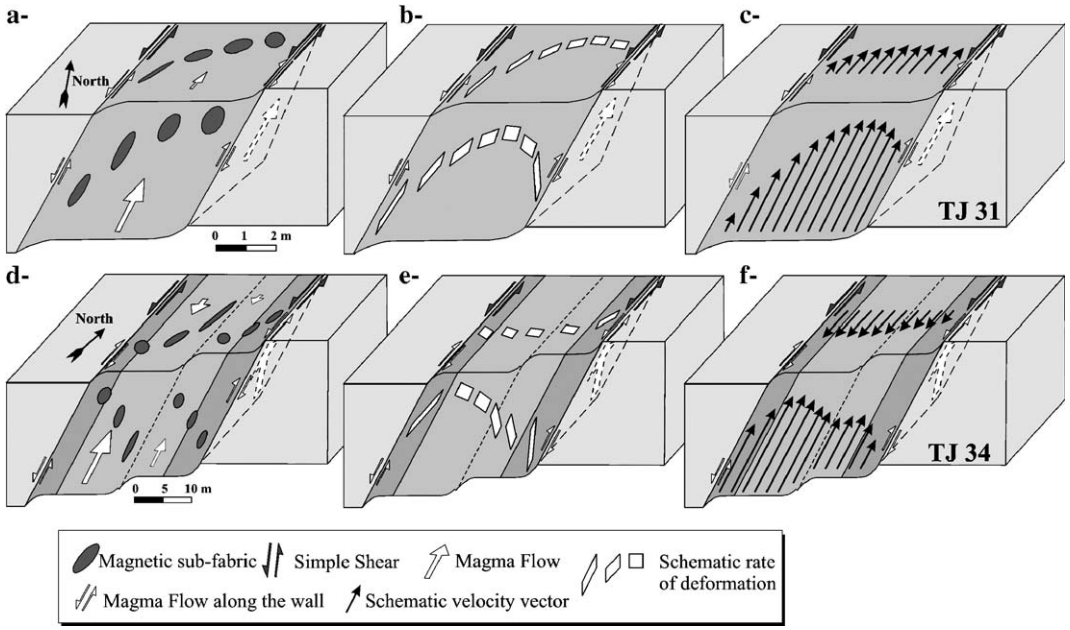

Fig. 10. Schematic sketches illustrating the relationship between the magnetic sub-fabric (a and d), the rate of deformation versus the dynamic of the wall rocks (b and e), and the related flow velocity vector profiles (c and f) for TJ31 and TJ34 dykes.

magma corresponding to the transition from a Newtonian to a Bingham-type behaviour related to the increase of solid particles (phenocrysts) by Bagnold effect (see §7.2) during emplacement of the dyke. Simultaneously, the lateral magmatic strain induced the decrease of P' by particle interaction outside this preserved central domain. Interactions between particles in a Newtonian medium result from the relative translation movement of crystals in the shear strain path, inducing irregular rotation of the particles. This destroys the periodicity of the shape fabric and induces low fabric intensity (Arbaret et al., 1996, 1997). This phenomenon is recorded in the studied dykes in the biotite-bearing external zones as well as in the eastern

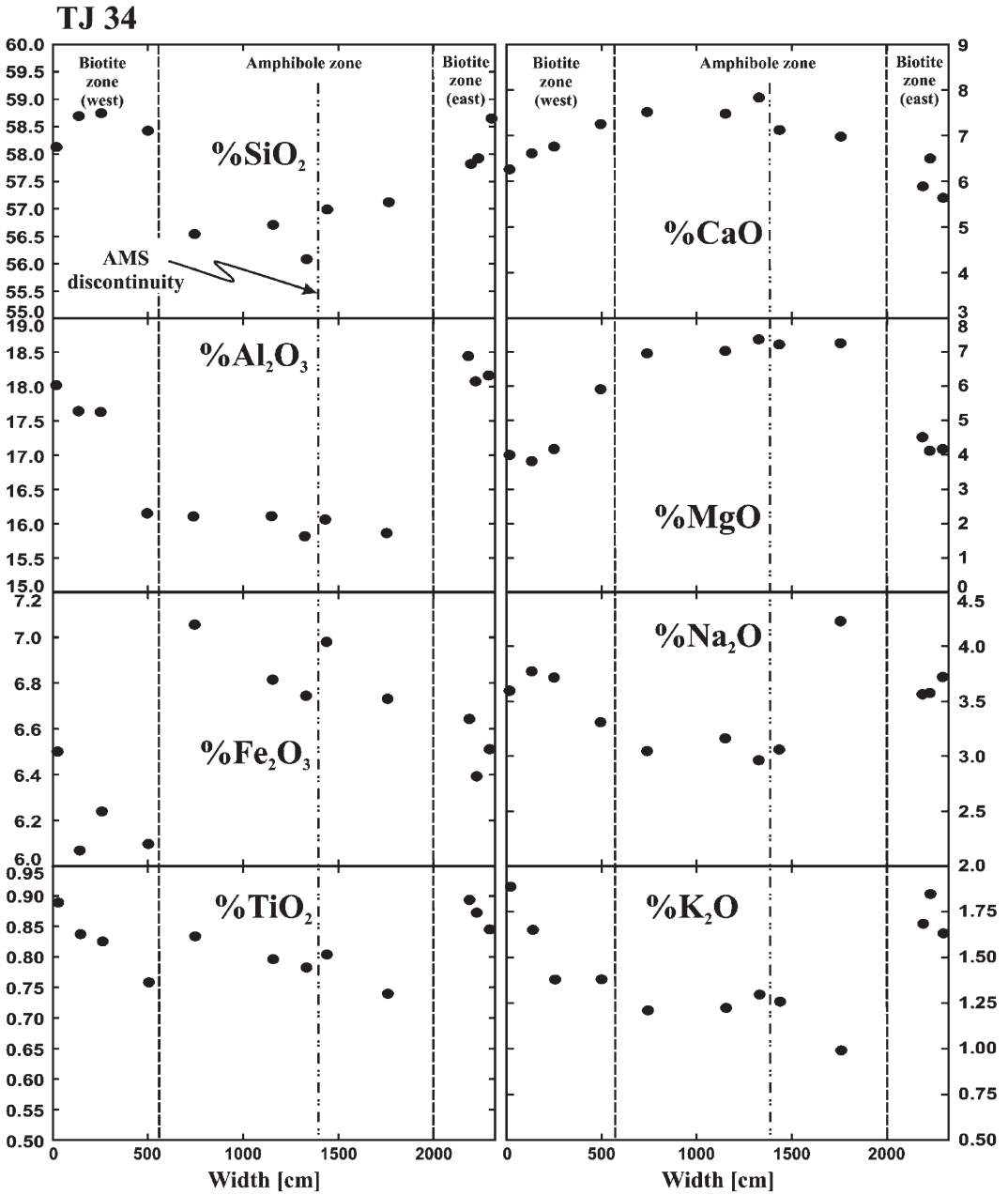

Fig. 11. Major element oxides (in wt.%) vs. width (in cm) for whole-rock samples of the TJ34 basaltic andesite dyke. Note that the core has lower SiO_2, Al_2O_3, Na_2O, K_2O and higher Fe_2O_3t, MgO and CaO contents than the margins. TJ34q (1810 cm) has an abnormally high Na_2O content and abnormally low K_2O content suggesting a more pronounced local albitisation of the rocks.

part of the amphibole zone. These zones thus had a Newtonian magma behaviour in which the flow was collected around a Bingham plug (western amphibole zone).

5.2.3. Magnetic foliation and lineation

The axes of the AMS ellipsoids have very regular orientations in the two dykes. The stereographic projections of the foliation and lineation have been plotted (Fig. 10) after tilting the wall to a vertical position. The patterns of magnetic foliations K_1K_2 (perpendicular to K_3 magnetic direction) and lineations K_1 are thus roughly homogeneous and exclude the presence of a single domain magnetite of inverse fabric (Rochette et al., 1992) in the retrogressive zone of TJ34. However, these orientations are unusual for dykes, which generally show imbricate foliation near the walls and inverse fabric in the core (Callot et al., 2001; Geoffroy et al., 2002; Callot and Guichet, 2003). In the MDS, the dykes are characterized by oblique sigmoid foliation trajectories (Fig. 9) and show local concave or convex morphologies near dyke boundaries that have been also observed in the field (penetrative and curved cleavage along the walls in the chilled margin without associated deformation of the country rocks). These foliation trajectories are indicative of a sinistral transcurrent movement (Féménias et al., 2004) recorded during the magmatic emplacement of the dykes (Correa-Gomes et al., 2001) and during the last increments of the solid-state deformation along the walls.

Moreover, the AMS lineations do not correspond to the deep line in the magnetic plane everywhere (the plunge varies from 52° to 87° for TJ34 and from 45° to 88° for TJ31), which implies a horizontal component of the magmatic flow. Some of the low plunge values (< 60°) are closed to dyke boundaries of TJ31 and, to a lesser extent, of the eastern rim of TJ34 also. On the contrary, in the central part of the dykes, lineations are concentrated around a position down the dip of the foliation (Fig. 8a; vertical after tilting of the wall in Fig. 9) and record slight variations of the flowing regime. This structural pattern across the dykes is representative of a more or less homogeneous vertical magmatic flow that is preserved in the core while a superposed lateral sinistral movement of the wall is clearly recorded near dyke boundary where the vertical flow is deviated.

In Fig. 10, we have tried to model the flow trajectories responsible of the structural pattern deduced from the AMS survey: 1) the magnitude of the ellipsoid of the fabric estimated from the relationship between P' and T (Fig. 10a and d); 2) the rate of deformation deduced from the orientation of the flow (Fig. 10b and e). For TJ31 (Fig. 10a and b) we consider an evolution of the flow with an

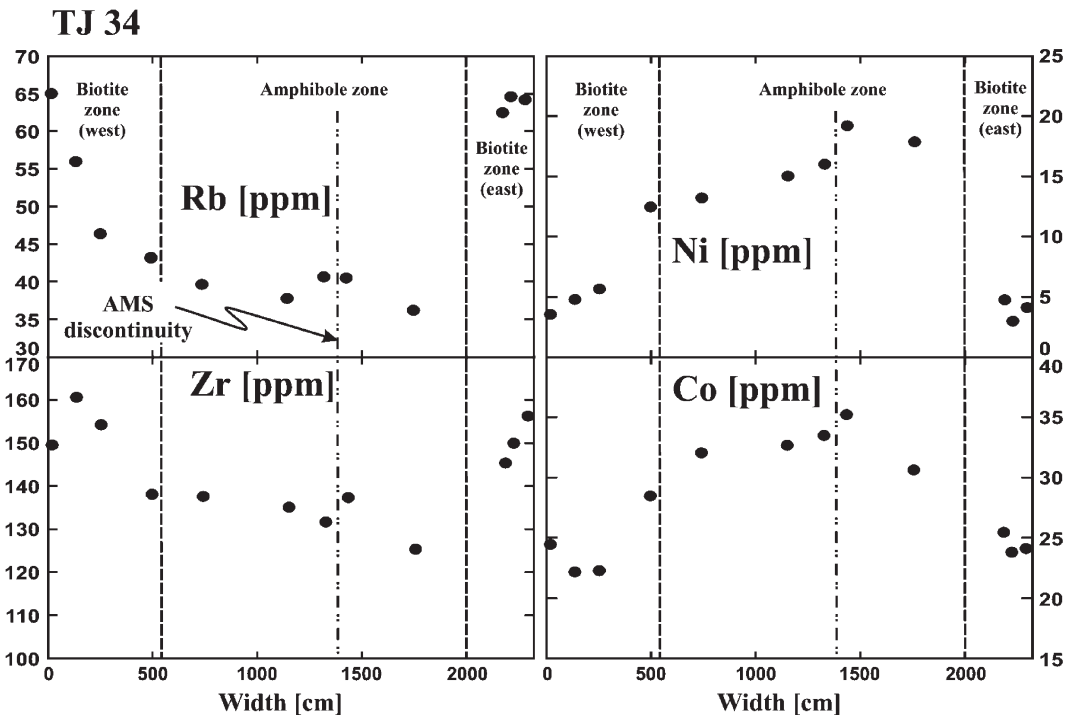

Fig. 12. Trace elements (in ppm) vs. width (in cm) for whole-rock samples of the TJ34 basaltic andesite dyke.

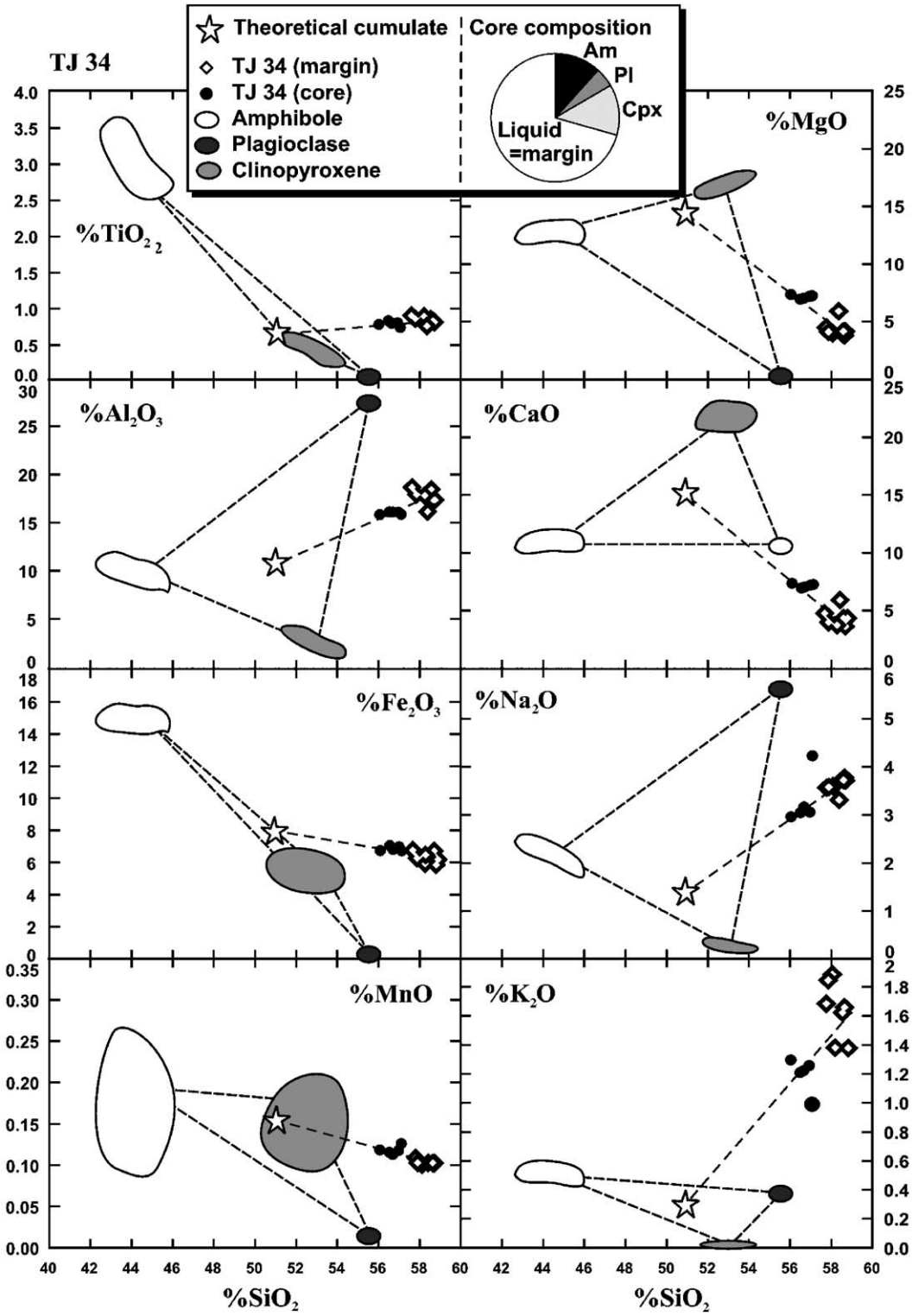

Fig. 13. Major element oxides versus SiO_2 (in wt.%) diagrams for the main phenocrysts (clinopyroxene, amphibole and plagioclase; data from Féménias, 2003) and whole-rock samples for the dyke TJ34. The dashed triangle limits the composition domain of the total solid phases involved in the fractional crystallization process. The dashed grey line illustrates the mass balance calculation allowing the evolution of the dyke from the central zone (core sample) to the margin by subtraction of theoretical cumulate. The white star represents the composition of this cumulate.

asymmetric profile and a maximum strain recorded at the eastern boundary. The pattern is more complex in TJ34 in which a rheological difference in the amphibole zone generated a kinematic step between a Bingham plug (western amphibole domain) and the Newtonian behaviour of the eastern part (which includes the eastern amphibole zone and the rich biotite rim).

6. Geochemistry of the TJ34 dyke

Bulk-rock chemical analyses (major and some trace elements) have been obtained for representative samples of the amphibole- and biotite-bearing zones of the TJ34 dyke. Twelve samples have been chosen covering both the petrographic (including CSD) and magnetic heterogeneities observed along the profile (Table 3).

6.1. Lateral chemical variations across the dyke

Plots of the major element concentrations vs. distance from the western wall of the dyke (Fig. 11) illustrate the differences of whole-rock compositions between the amphibole-bearing central zone and the biotite-bearing external margins. These chemical variations are well correlated with the petrographic observations: the high Fe_2O_3t, MgO, and CaO contents in the core reflect the presence of microphenocrysts (brown amphibole, plagioclase and clinopyroxene) whereas K_2O enrichment on the margins is correlated with the presence of biotite. In terms of magmatic composition, the core appears slightly but significantly, less evolved than the two biotite-bearing margins. The core was basaltic andesite whereas the margins have andesitic compositions (Fig. 3). The few samples from the transition zone have intermediate composition. Like the variations of the amphibole modal proportion, the distribution of most oxides in the central amphibole-bearing core is roughly asymmetrical. Moreover, a more or less well-pronounced step occurs in the element profiles at a width of 1400 cm (between stations TJ34n and TJ34o) where the AMS structural discontinuity has been observed.

The incompatible trace elements (Fig. 12) are significantly enriched in the margins of the dykes (i.e. Rb and Zr) when compared to the core. These elements are thus positively correlated with the SiO_2 content that ranges from ~56% in the core to ~59% in the margins. By contrast, most transition elements (Co, Cu, Ni), except Zn, show a significant enrichment in the central amphibole-bearing zone. These elements are positively correlated with the MgO, Fe_2O_3t and CaO contents and, by extension, to the amphibole and clinopyroxene modal proportions.

In the central amphibole-bearing core of the dyke, most trace elements (incompatible or compatible) display an asymmetrical distribution (i.e. Zr in Fig. 12) in agreement with asymmetrical petrological characteristics of the central zone. Moreover, there seems to be a step in the concentration profile at a width of 1400 cm (between station TJ34n and TJ34o), corresponding to the AMS structural discontinuity.

6.2. Magmatic differentiation: chemical modeling

Chemical variations of major and trace element contents across the dyke suggest a slight but significant magmatic differentiation that necessarily occurred inside the dyke body during flow. The margins, petrographically described as a liquid, are chemically more evolved and enriched in LIL and HFS elements whereas the core that contains amphibole, plagioclase and clinopyroxene microphenocrysts is interpreted as a crystal-laden liquid with more primitive composition (enrichment in compatible/transition element). The differentiation process that generated the core and the margins of the dyke can be tested quantitatively by a simple mass balance calculation. We check if the average chemical composition of the margin of the dyke can be obtained by fractionation (mechanical segregation) of amphibole, plagioclase and clinopyroxene. We also calculate the bulk composition of the interstitial microcrystalline material in the porphyritic core of the dyke. It is therefore possible to estimate the bulk composition of the fractionated solid phases (theoretical cumulate) as well as the modal proportions of the solid phases and of the liquid in the central mush.

Mass balance calculations (R is close to 0.55) suggest that the core composition corresponds to an assemblage of 12% amphibole + 5% of plagioclase + 13% of clinopyroxene ($\sum$crystals = 30%) and 70% of liquid, represented by the average composition of the margins of the dyke (Fig. 13). These calculated proportions are in good agreement with the observed modes.

7. Discussion

7.1. Petrographic and structural characteristics of the dykes

The TJ31 dyke (5.5 m thick) is an asymmetrical body as shown by the petrographic and structural data. The CSD of amphibole phenocrysts shows that the modal proportion varies strongly across dyke's width. The distribution of all the CSD parameters is asymmetrical and defines a long western half-dyke and a short eastern

half-dyke. The AMS results also display an asymmetrical fabric in particular oblique sigmoid magnetic foliation and lineation trajectories (Fig. 9). The peculiar relations between foliations, lineations and AMS shape parameters (P' and T) have been discussed in terms of the interaction between magma flow and the wall's tectonic displacement (Féménias et al., 2004). The axes of the finite deformation thus describe a mirror image of the magma velocity inside the dyke during the late stage of emplacement (Fig. 10). The lack of a clear inverse fabric argues for a fabric representative of the flow (Féménias et al., 2004). The south to north horizontal component of the magma flow, inferred from the direction and plunge of lineations near the walls, can be interpreted as the flow deviation during a horizontal sinistral component of the tectonic movement of the walls deduced from the asymmetrical foliations. This velocity profile across the dyke logically displays an asymmetrical shape, in agreement with the amphibole size and abundance distribution (Figs. 5 and 7).

The thicker TJ34 dyke (23 m) is more complex. It is globally symmetrical with biotite zones on each side of the central amphibole zone but it displays local asymmetrical petrographic and structural characteristics. The two types of patterns (asymmetrical and symmetrical) are nevertheless roughly correlated with the AMS parameters and with the fabric of the body. The petrographic discontinuities between the central amphibole-bearing and the external biotite-bearing zones are correlated with significant structural changes (Fig. 9; lineation and foliation slopes). The asymmetrical profiles of the amphibole CSD parameters (e.g., modal proportion, sizes, etc.) indicate an off centre petrographic core, i.e. close to the western amphibole–biotite boundary. The AMS shape parameters (P' and T) record the same asymmetry. The axes of the finite deformation

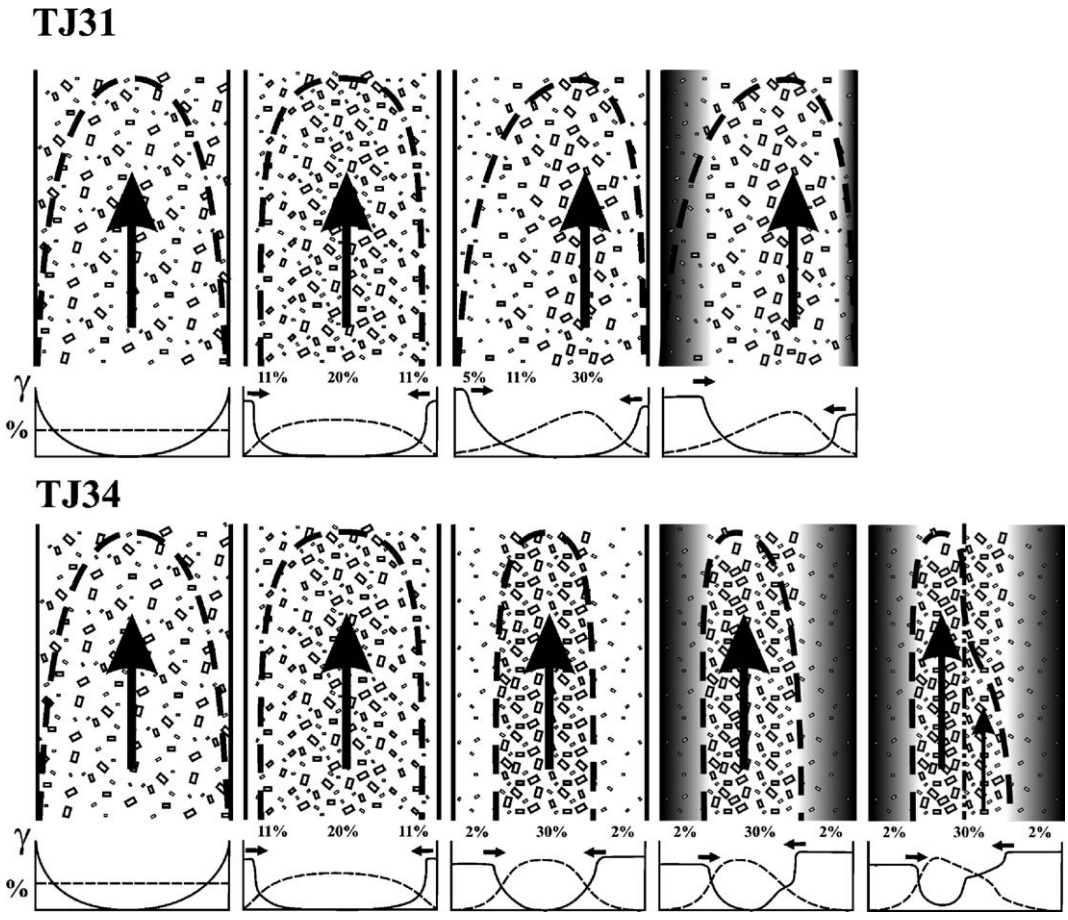

Fig. 14. Evolution of the crystals distribution during the emplacement and cooling of the dykes. Below each sketch, the diagram qualitatively shows the amount of crystals (dashed line) and the evolution of the deformation rate γ (solid line) through the dyke. For both the right part of the figure illustrates the finite state of each dyke. The Bagnold effect is responsible for the segregation of crystals in the core and the formation of crystal-free margins (in grey).

describe a mirror image of the magma velocity inside the dyke during the late stage of emplacement (Fig. 10).

7.2. Crystal migration inferred by the Bagnold effect

The amphibole microphenocrysts (Ti-rich pargasite-tschermakite) crystallize at high $T°$ (900–1100 °C) and high P (0.45–0.7 GPa) in a deep magma chamber before the sub-surface emplacement of the magma in the dykes. CSD and AMS record the same dynamic process. Indeed in a simple sheet of magma (like a dyke), the shear field varies across the dyke's width, from a maximum value (γ in Fig. 14) near the walls (slow down velocity of flow) to zero at the centre (maximum velocity of flow). Scale experiments designed to reproduce the flow of magma suspensions during ascent and emplacement have been made by Bhattacharji (1967). The experiments show that flow is accompanied by axial migration of solids towards the centre of the flow (the Bagnold effect; Bagnold, 1954), even for relatively low (15% by volume) particle contents. Despite being a purely phenomenological description, the Bagnold effect is cited as the dominant mechanism for flow segregation of crystals or other suspended material commonly observed in solidified dykes and sills (e.g., Komar, 1972a,b; Barrière, 1976; Philpotts, 1990).

Although the CSD of amphibole displays classical patterns and a fanning distribution, the interpretation of these data could not be linked to a simple static cooling/growth process. In our opinion, the intercept number ($n°$) is not only an approximation of the nucleation rate during static cooling. As the strain intensity and the importance of the Bagnold effect (Bagnold, 1954) depend on the distance to the wall of the dyke, the mean crystal length (Lm), the total number of grains (N_T) and the line parameters (S and $n°$) change naturally along the velocity profile. The biotite of the marginal zones of the dyke crystallized at significantly lower $T°$ (600–680 °C) than the amphibole of the central zone, suggesting that it formed during the cooling of the dyke in subvolcanic environment. So the CSD of the biotite can reasonably be linked to the static crystallization occurring late in the cooling history of a more evolved liquid.

7.3. Behaviour of the magma during the ascent to its emplacement

The migration of crystals inside a dyke is an integral factor in the rheological behaviour of magma during its emplacement. In magma carrying moderate (10 to 30%) proportion of suspended crystal, viscous fluctuations may lead to flow differentiation by shear-enhanced diffusion (Petford, 2003). In the studied Motru dykes, the high proportion of liquid near the margins of the dyke implies a steady state flow characterized by a Newtonian behaviour of the fluid as long as the liquid/glass transition is not reached. This Newtonian behaviour is no more possible in the core zone where the amount of suspended crystals reaches the threshold values of 30–40%. The margins of the dyke are thus lubricated channel where the flow is localized, whereas the core behaves like a Binghamian plug (Fig. 14). The localization of this Newtonian liquid on both margins of the dyke has certainly facilitated the ascent of the central Binghamian mush during the dyke emplacement. The structural step (AMS) observed in the central part of the TJ34 body (Figs. 9 and 10) would correspond to the last kinematic effects recorded in an almost completely solidified dyke (dissociation of the plug into two bodies of contrasted velocity) This structural step is observable on the chemical profiles as a "fault map effect".

8. Conclusion

The Motru Dyke Swarm intrudes the late-Pan-African units of the Danubian window in the Southern Carpathians of Romania. The dykes form a subvolcanic high-K calc-alkaline series that mainly consist of basaltic andesites and basalts. The rocks are aphyric to micro-porphyritic with amphibole (Ti-pargasite-tschermakite), clinopyroxene and plagioclase (both strongly retrogressed) microphenocrysts.

Two dykes (5.5 m and 24 m thick) have been studied in details. Their amphibole phenocrysts crystallized at high T–high P (900–1100 °C; 0.4–0.7 GPa), i.e. in a deep magma chamber before dyke emplacement in a subvolcanic environment.

Crystal size distribution (CSD) and magnetic (AMS) structural data obtained on series of samples cored along dyke's width give concordant results and record the same dynamic process. The microphenocrysts that predate the dyke emplacement were segregated (Bagnold effect) during magma ascent and emplacement at high level.

From a rheological point of view, this segregation is responsible for the formation of (1) a crystal-rich core zone (crystal mush) that behaves as a Binghamian fluid and (2) crystal-free margins (liquid) that behave as a Newtonian fluid and localized the deformation during magma ascent. The mineral segregation induces a small but significant magmatic differentiation (flowage differentiation)

between core and margins in the thicker dyke: the core is enriched in compatible (Mg, Fe, Ca, Ni, Co) and the margins in incompatible (K, Zr, Rb, etc.) elements.

Acknowledgments

This work was partly supported by a grant from NATO for the field survey. We wish to thank J.P. Callot and two anonymous reviewers for their careful and fruitful comments. The suggestions of Dr. M. Mangan (Chief Editor) are also gratefully acknowledged. Magnetic measurements (AMS) were supported by CLDG La Rochelle. We also thank M.D. Higgins who provided us with the last version of the CSDCorrection 1.36 software and C. Walter who revised the English language.

References

Arbaret, L., Diot, H., Bouchez, J.L., 1996. Shape fabrics of particles in low concentration suspensions: 2D analogue experiments and application to tiling in magma. Journal of Structural Geology 18 (7), 941–950.

Arbaret, L., Diot, H., Bouchez, J.L., Saint Blanquat, M., Lespinasse, P., 1997. Analogue 3D simple shear experiments of magmatic biotite subfabric. In: Bouchez, J.L., Hutton, D.H.W., Stephens, W.E. (Eds.), Granites: From Segregation of Melt to Emplacement Fabrics. Kluwer Academic Publishers, Dordrecht, pp. 129–143.

Archanjo, C.J., Trindade, R.I., Macedo, J.W.P., Araújo, M.G., 2000. Magnetic fabric of a basaltic dyke swarm associated with Mesozoic rifting in northeastern Brazil. Journal of South American Earth Sciences 13, 179–189.

Bagnold, R.A., 1954. Experiments on a gravity-free dispersion of large solid spheres in a Newtonian fluid under shear. Proceeding of the Royal Society of London 225, 49–63.

Barrière, M., 1976. Flowage differentiation; limitation of the "Bagnold effect" to the narrow intrusions. Contributions to Mineralogy and Petrology 55 (2), 139–145.

Berza, T., Seghedi, A., 1975. Complexul filonian presilurian din bazinul Motrului (Carpaţii Meridionali). D.S. Inst. Geol. Geofiz. LXI/1, 131–149.

Bhattacharji, S., 1967. Mechanics of flow differentiation in ultramafic and mafic sills. Journal of Geology 75, 101–111.

Bhattacharji, S., Hehru, C.E., 1972. Igneous Differentiation Models for the Origin of Mount Johnson, a zoned Monteregian Intrusion, vol. 14. I G C, Quebec, Canada, pp. 3–17.

Bhattacharji, S., Smith, C.H., 1964. Flowage differentiation. Geological Survey of Canada 145, 150–153.

Callot, J.P., Guichet, X., 2003. Rock texture and magnetic lineation in dykes: a simple analytical model. Tectonophysics 366, 3–4, 15, 207–222.

Callot, J.P., Geoffroy, L., Aubourg, C., Pozzi, J.P., Mege, D., 2001. Magma flow of shallow dykes from the East Greenland volcanic margin inferred from magnetic studies. Tectonophysics 335, 313–329.

Cañón-Tapia, E., Walker, G.P.L., Herrero-Bervera, E., 1996. The internal structure of lava flows—insights from AMS measurements I: near-vent a'a. Journal of Volcanology and Geothermal Research 70, 21–36.

Cashman, K.V., 1992. Groundmass crystallization of Mount St. Helens dacite, 1980–1986: a tool for interpreting shallow magmatic processes. Contributions to Mineralogy and Petrology 109, 431–449.

Cashman, K.V., 1993. Relationship between plagioclase crystallization and cooling rate in basaltic melts. Contributions to Mineralogy and Petrology 113, 126–142.

Cashman, K.V., Marsh, B.D., 1988. Crystal Size Distribution (CSD) in rocks and the kinetics of crystallization II: Makaopuhi lava lake. Contributions to Mineralogy and Petrology 99, 292–305.

Correa-Gomes, L.C., Souza Filho, C.R., Martins, C.J.F.N., Oliveira, E. P., 2001. Development of symmetrical and asymmetrical fabrics in sheet-like igneous bodies: the role of magma flow and wall-rock displacements in theoretical and natural cases. Journal of Structural Geology 23, 1415–1428.

Féménias, O., 2003. Contribution à l'étude du magmatisme tardi-à post-orogénique. De sa source à sa mise en place en sub-surface: exemples régionaux de l'essaim de filons du Motru (Roumanie) et du complexe lité profond sous Beaunit (France). PhD Thesis Université Libre de Bruxelles. 450 pp.

Féménias, O., Diot, H., Berza, T., Gauffriau, A., Demaiffe, D., 2004. Asymmetrical to symmetrical magnetic fabric of dikes: paleo-flow orientations and paleo-stresses recorded on feeder-bodies from the Motru Dike Swarm (Romania). Journal of Structural Geology 26, 1401–1418.

Féménias, O., Mercier, J.-C.C., Nkono, C., Diot, H., Berza, T., Tatu, M., Demaiffe, D., 2006. Calcic amphibole growth and compositions in calc-alkaline magmas: evidence from the Motru Dyke Swarm (Southern Carpathians, Romania). American Mineralogist 91, 73–81.

Fernandez, A., Laporte, D., 1991. Significance of low symmetry fabrics in magmatic rocks. Journal of Structural Geology 13, 337–347.

Geoffroy, L., Callot, J.P., Aubourg, C., Moreira, M., 2002. Magnetic and plagioclase linear fabric discrepancy in dykes: a new way to define the flow vector using magnetic foliation. Terra Nova 14, 183–190.

Higgins, M.D., 1996. Magma dynamics beneath Kameni volcano, Thera Greece, as revealed by crystal size and shape measurements. Journal of Volcanology and Geothermal Research 70, 37–48.

Higgins, M.D., 2000. Measurement of crystal size distribution. American Mineralogist 85, 1105–1116.

Higgins, M.D., 2002. Closure in crystal size distribution (CSD), verification of CSD calculation and the significance of CSD fans. American Mineralogist 87, 160–164.

Hrouda, F., 1982. Magnetic anisotropy of rocks and its application in geology and geophysics. Geophysical Survey 5, 37–82.

Irvine, T.N., Baragar, W.R.A., 1971. A guide to the chemical classification of the common volcanic rocks. Canadian Journal of Earth Sciences 8, 523–548.

Jelinek, V., 1981. Characterization of the magnetic fabric of the rocks. Tectonophysics 79, 63–67.

Knight, D., Walker, M., 1988. Magma flow direction in dykes of Koolau Complex, Oahu, determined from magnetic fabric studies. Journal of Geophysical Research B5, 4301–4319.

Komar, P.D., 1972a. Mechanical interactions of phenocrysts and flow differentiation of igneous dykes and sills. Geological Society of America Bulletin 83, 973–988.

Komar, P.D., 1972b. Flow differentiation in igneous dykes and sills; profiles of velocity and phenocryst concentration. Geological Society of America Bulletin 83, 3443–3447.

Komar, P.D., 1976. Phenocryst interactions and the velocity profile of magma flowing through dykes or sills. Geological Society of America Bulletin 87 (9), 1336–1342.

Leake, B.E., Woolley, A.R., Arps, C.E.S., Birch, W.D., Gilbert, M.C., Grice, J.D., Hawthorne, F.C., Kato, A., Kisch, H.J., Krivovichev, V.G., Linthout, K., Laird, J., Mandarino, J., Maresch, W.V., Nickel, E.H., Rock, N.M.S., Schumacher, J.C., Smith, D.C., Stephenson, N.C.N., Ungaretti, L., Whittaker, E.J.W., Youzhi, G., 1997. Nomenclature of amphiboles: report of the Subcommittee on Amphiboles of the International Mineralogical Association Commission on new minerals and mineral names. Mineralogical Magazine 61, 295–321.

Le Bas, M.J., Le Maître, R.W., Streckeisen, A., Zanettin, B., 1986. A chemical classification of volcanic rocks based on the total alkali-silica diagram. Journal of Petrology 27, 745–750.

Le Maitre, R.W. (Ed.), 2002. Igneous Rocks. A Classification and Glossary of Terms, 2nd ed. IUGS-Cambridge Univ. Press. 236 pp.

Mangan, M.T., 1990. Crystal size distribution systematics and the determination of magma storage times: the 1959 eruption of Kileuea volcano, Hawaii. Journal of Volcanology and Geothermal Research 44, 295–302.

Mangan, M.T., Marsh, B.D., 1992. Solidification front fractionation in phenocryst-free sheet-like magma bodies. Journal of Geology 100, 605–620.

Marsh, B.D., 1988. Crystal size distribution (CSD) in rocks and the kinetics and dynamics of crystallization; theory. Contributions to Mineralogy and Petrology 99, 277–291.

Marsh, B.D., 1998. On the interpretation of crystal size distribution in magmatic systems. Journal of Petrology 39, 553–599.

Marsh, B.D., Liu, T., 1999. Ridge magmatism: Atlantic vs. Pacific as recorded by crystal size distribution (CSDs). EOS Transactions, American Geophysical Union 80, S311.

Mock, A., Jerman, D.A., Breitkreuz, C., 2003. Using quantitative texture analysis to understand the emplacement of shallow-level rhyolitic laccoliths: a case study from the Halle volcanic complex, Germany. Journal of Petrology 44, 833–849.

Nicolas, A., 1992. Kinematics in magmatic rocks with special reference to gabbros. Journal of Petrology 33, 891–915.

Petford, N., 2003. Rheology of granitic magmas during ascent and emplacement. Annual Review Earth and Planetary Sciences 31, 399–427.

Philpotts, A.R., 1990. Principles of Igneous and Metamorphic Petrology. Prentice-Hall, Englewood Cliffs, N.J. 498 pp.

Raposo, M.I.B., D'Agrella-Filho, M.S., 2000. Magnetic fabrics of dyke swarms from SE Bahia State, Brazil: their significance and implications for Mesoproterozoic basic magmatism in the São Francisco Craton. Precambrian Research 99, 309–325.

Resmini, R.G., Marsh, B.D., 1995. Steady-state volcanism, paleoeffusion rates, and magma system volume inferred from plagioclase crystal size distributions in mafic lavas: Dome Mountain, Nevada. Journal of Volcanology and Geothermal Research 68, 273–296.

Rickwood, 1989. Boundary lines within petrologic diagrams which use oxides of major and minor elements. Lithos 22, 247–263.

Rochette, P., Jackson, M., Aubourg, C., 1992. Rock magnetism and the interpretation of anisotropy of magnetic susceptibility. Review of Geophysics 30, 209–226.

Sahagian, D.L., Proussevitch, A.A., 1998. 3D particle size distributions from 2D observations; stereology for natural applications. Journal of Volcanology and Geothermal Research 84, 173–196.

Saltikov, S.A., 1967. The determination of the size distribution of particles in an opaque material from a measurement of the size distribution of their sections. In: Elias, H. (Ed.), Proceeding of the Second International Congress from Stereology. Springer-Verlag, Berlin, pp. 163–173.

Winkler, H.G.F., 1949. Crystallization of basaltic magma as recorded by variation of crystal sizes in dykes. Mineralogical Magazine 28, 557–574.

Wones, D.R., Eugster, H.P., 1965. Stability of biotite: experiment, theory and application. American Mineralogist 50, 1228–1272.

Zieg, M.J., Marsh, B.D., 2002. Crystal size distribution and scaling laws in the quantification of igneous textures. Journal of Petrology 43, 85–101.